ADVANCED FUNCTIONAL MATERIALS

# Supporting Information

for *Adv. Funct. Mater.,* DOI: 10.1002/adfm.202302098

## Nanocellulose-Carboxymethylcellulose Electrolyte for Stable, High-Rate Zinc-Ion Batteries

*Lin Xu, Taotao Meng, Xueying Zheng, Tangyuan Li, Alexandra H. Brozena, Yimin Mao, Qian Zhang, Bryson Callie Clifford, Jiancun Rao, and Liangbing Hu**

# Supporting Information

## Nanocellulose-carboxymethylcellulose electrolyte for stable, high-rate Zinc-ion batteries

Lin Xu,[1] Taotao Meng,[1] Xueying Zheng,[1] Tangyuan Li,[1] Alexandra H. Brozena, [1] Yimin Mao,[1] Qian Zhang,[1] Bryson Callie Clifford, Jiancun Rao,[2] Liangbing Hu[1,*]

1. Department of Materials Science and Engineering, University of Maryland, College Park, Maryland, 20742
2. Advanced Imaging and Microscopy Laboratory, University of Maryland, College Park, MD 20742, United States

[*] Email: binghu@umd.edu

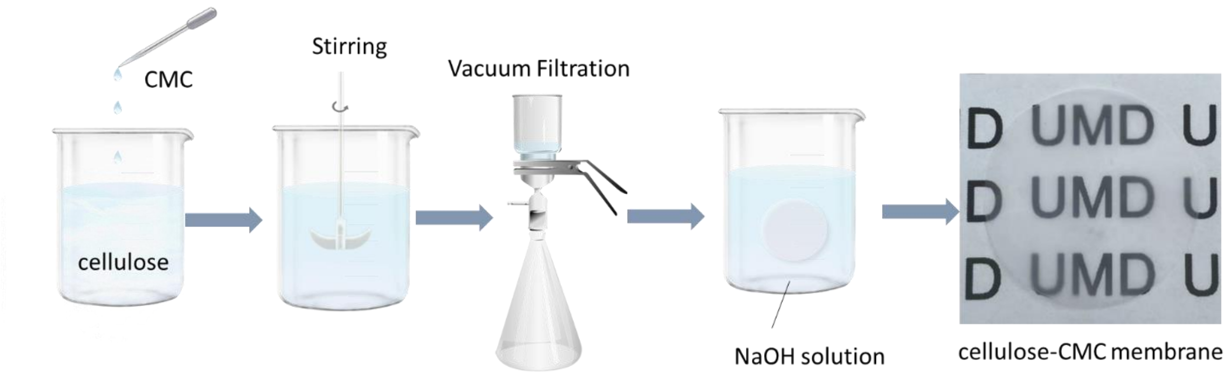


**Figure S1.** Schematic diagram of the preparation of the cellulose-CMC membrane.

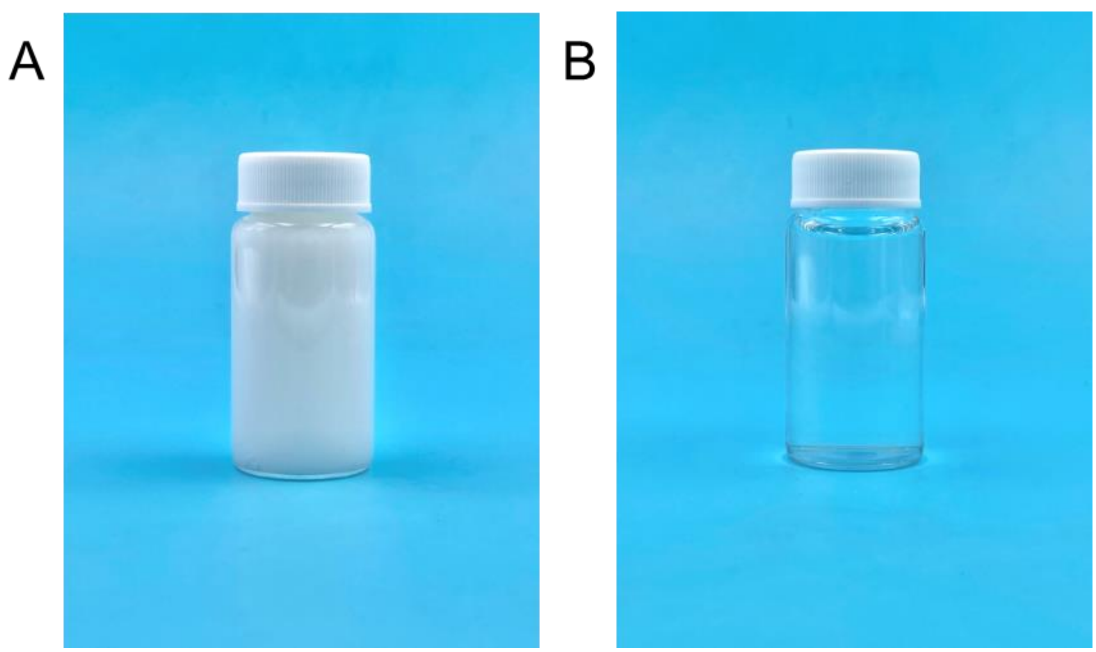


**Figure S2.** (A) The 3 wt% cellulose nanofiber gel and (B) 0.5 wt% CMC in water.

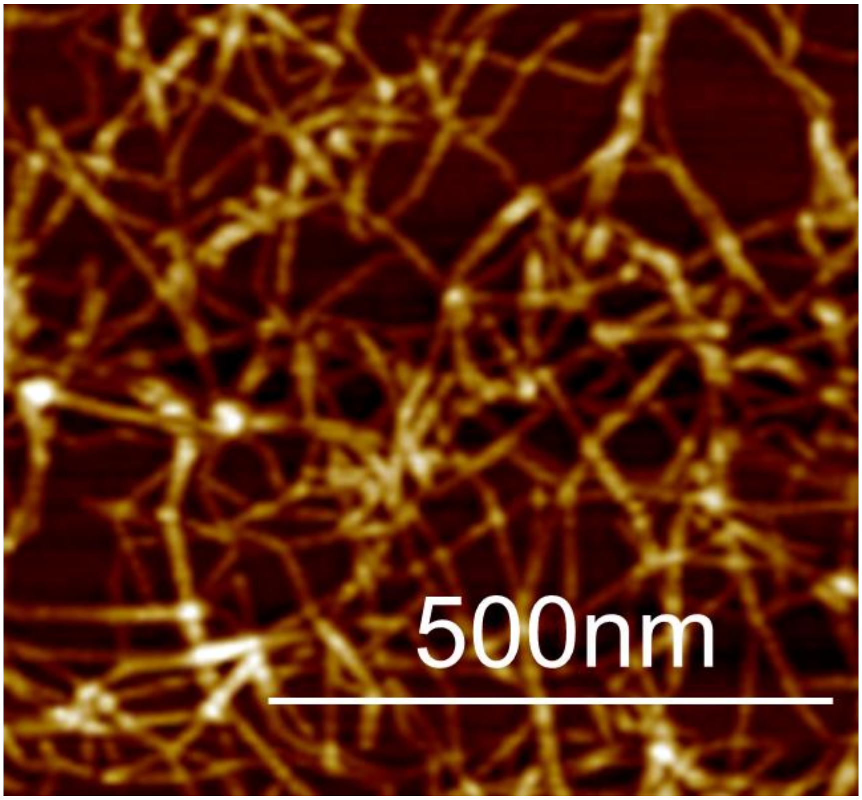


**Figure S3.** AFM characterization of the cellulose nanofibers, which feature diameters of tens of nanometers and lengths of several microns.

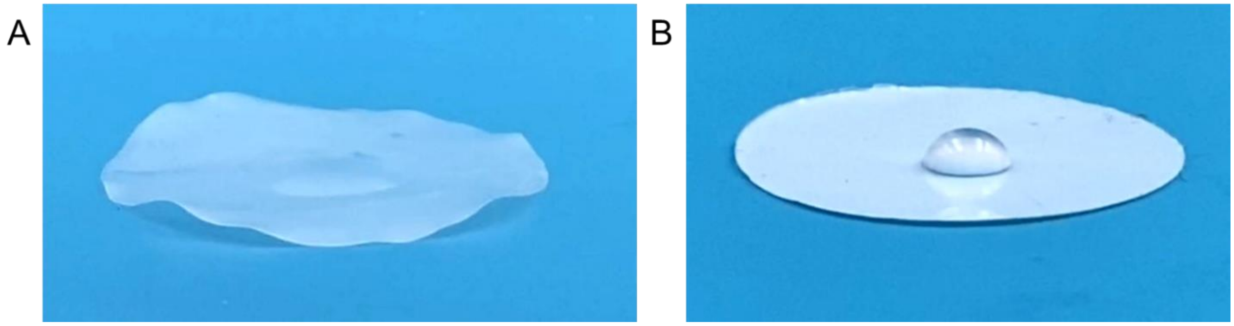


**Figure S4.** Surface contact angles of water on the (A) cellulose-5 wt% CMC electrolyte and (B) a commercial Celgard membrane. The cellulose-CMC electrolyte shows excellent hydrophilicity.

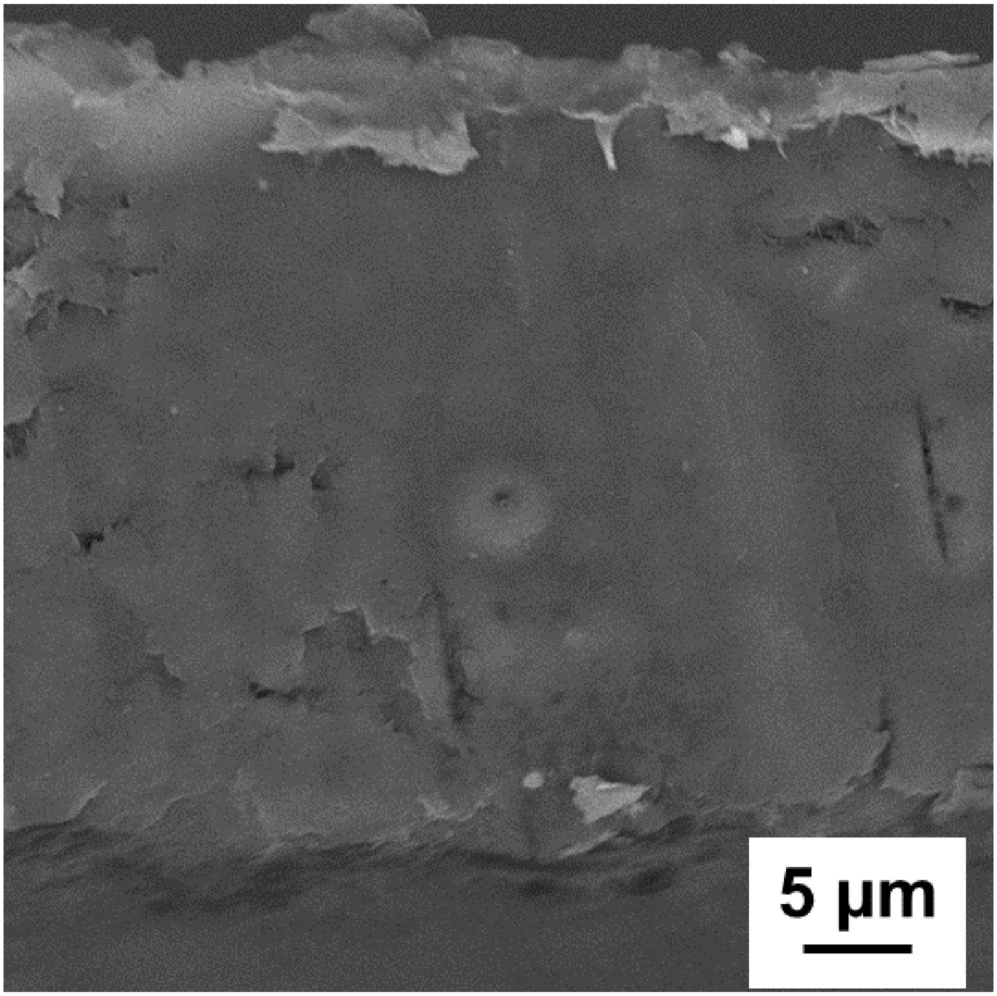


**Figure S5.** Cross-sectional SEM image of the cellulose-5% CMC membrane before the NaOH treatment, which exhibits a dense structure.

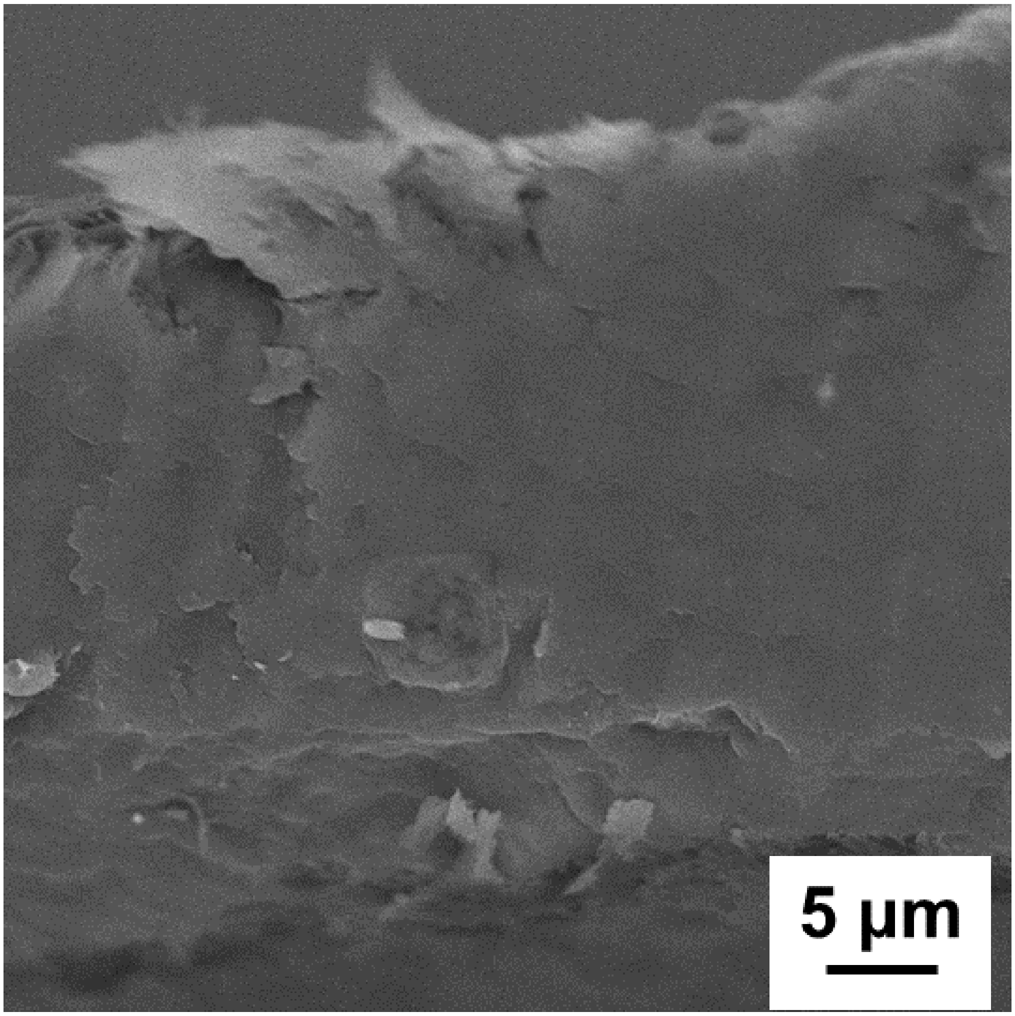


**Figure S6.** Cross-sectional SEM image of the cellulose-5% CMC membrane after the NaOH treatment, which still exhibits a dense structure.

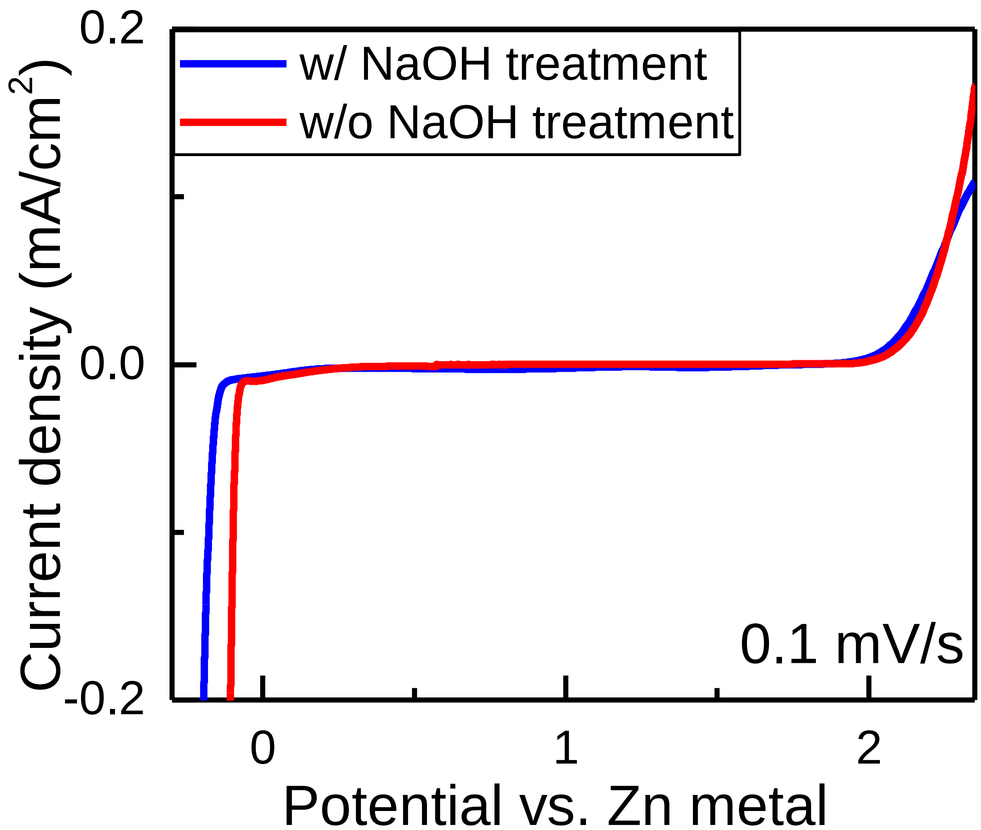


**Figure S7.** Electrochemical window of the cellulose-5 wt% CMC membrane before and after the NaOH treatment. No significant difference was observed.

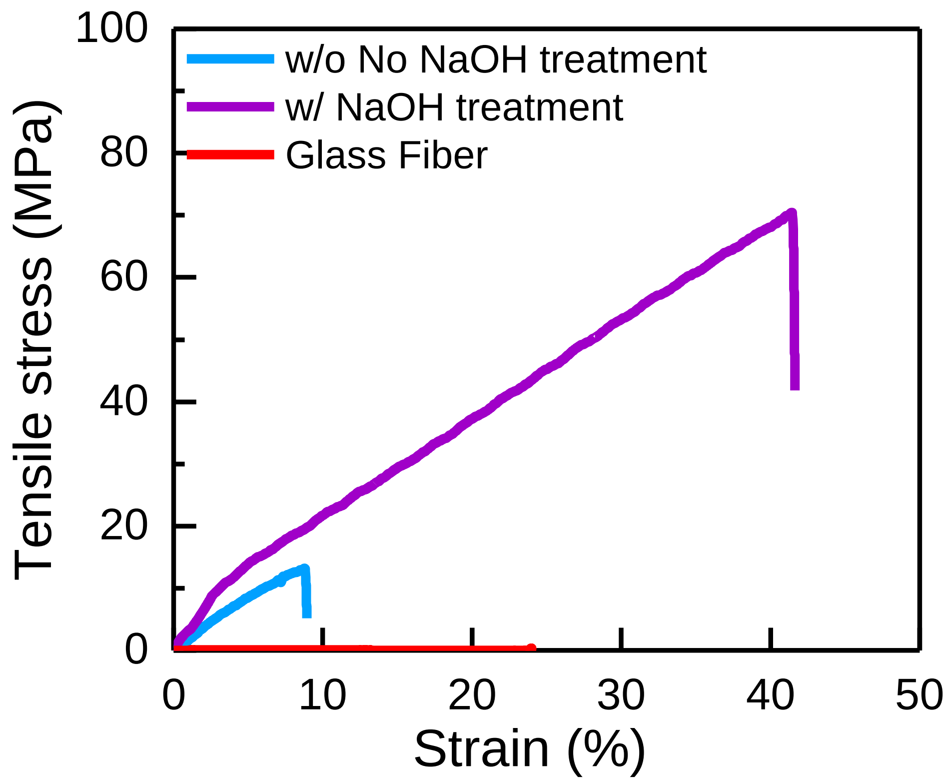


**Figure S8.** Tensile tests of the cellulose-5% CMC membrane before and after NaOH treatment, as well as a glass fiber separator as a control.

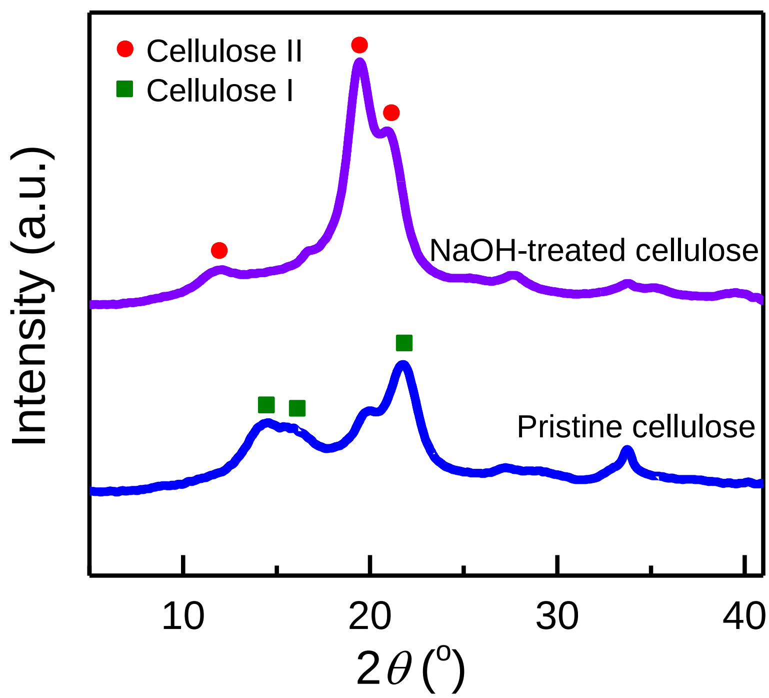


**Figure S9.** XRD patterns of the cellulose membrane before and after NaOH treatment.

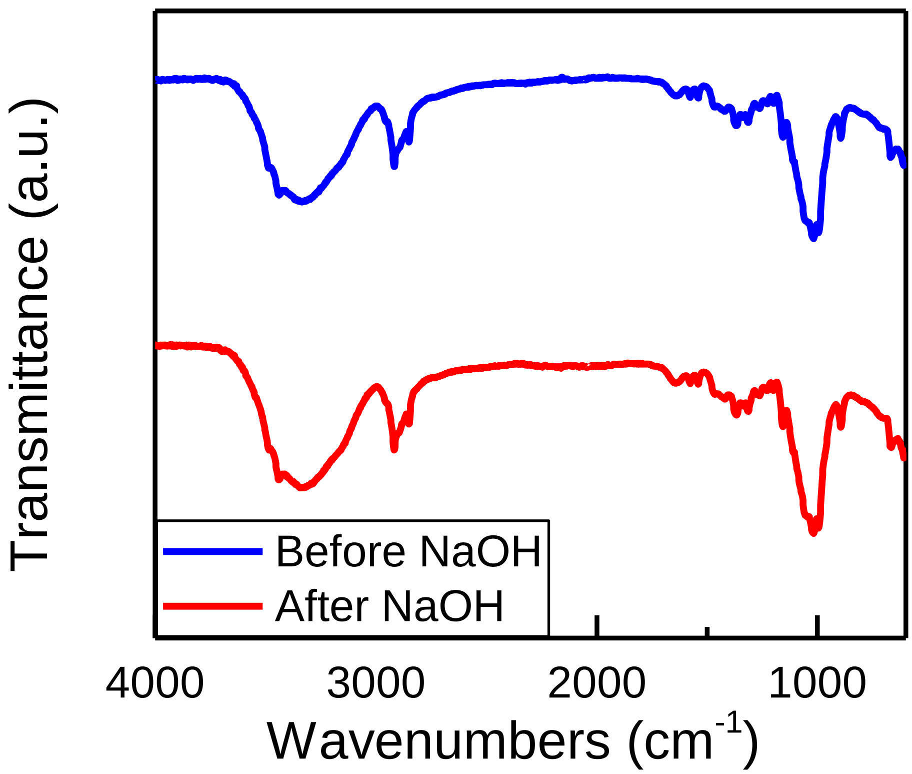


**Figure S10.** FTIR of the cellulose-5% CMC membrane before and after the NaOH treatment. No significant difference was observed.

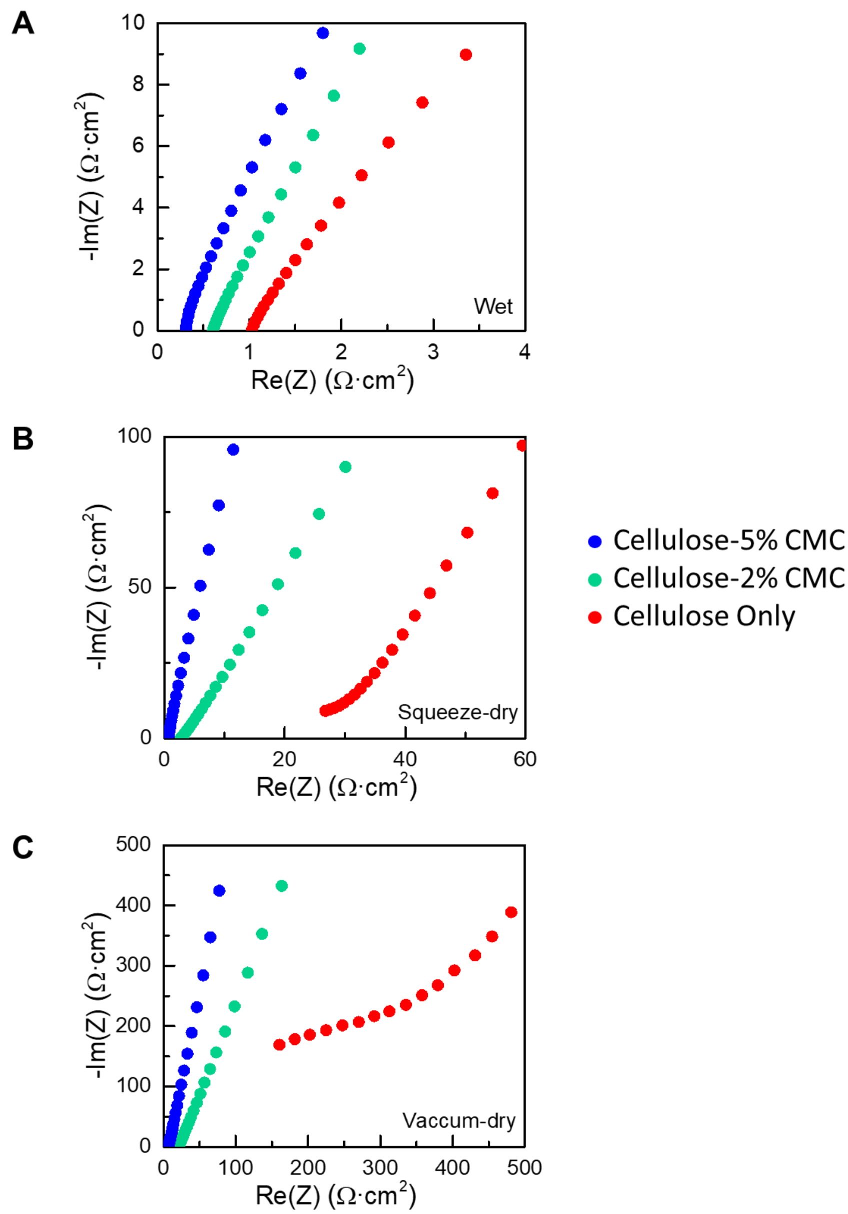


**Figure S11.** EIS of the cellulose-only (red), cellulose-2% CMC (green) and cellulose-5% CMC (blue) membranes with (A) wet measurement (B) squeeze-dry by Kimwipes using 0.5 MPa pressure (C) placed under vacuum for 30 s after squeeze-dry. The thicknesses of electrolytes were 80 μm.

**Table S1.** Percentage of water in the cellulose-only (0 wt% CMC), cellulose-2% CMC, and cellulose-5% CMC membranes under the different drying conditions, including the fully wet state, after squeeze-drying, and vacuum-drying.

| Percentage of CMC | Wet | Squeeze-dry | Vacuum-dry |
|---|---|---|---|
| 0% | 61 ± 3% | 30 ± 3% | 10 ± 1% |
| 2% | 63 ± 3% | 48 ± 4% | 25 ± 2% |
| 5% | 66 ± 5% | 60 ± 5% | 35 ± 2% |

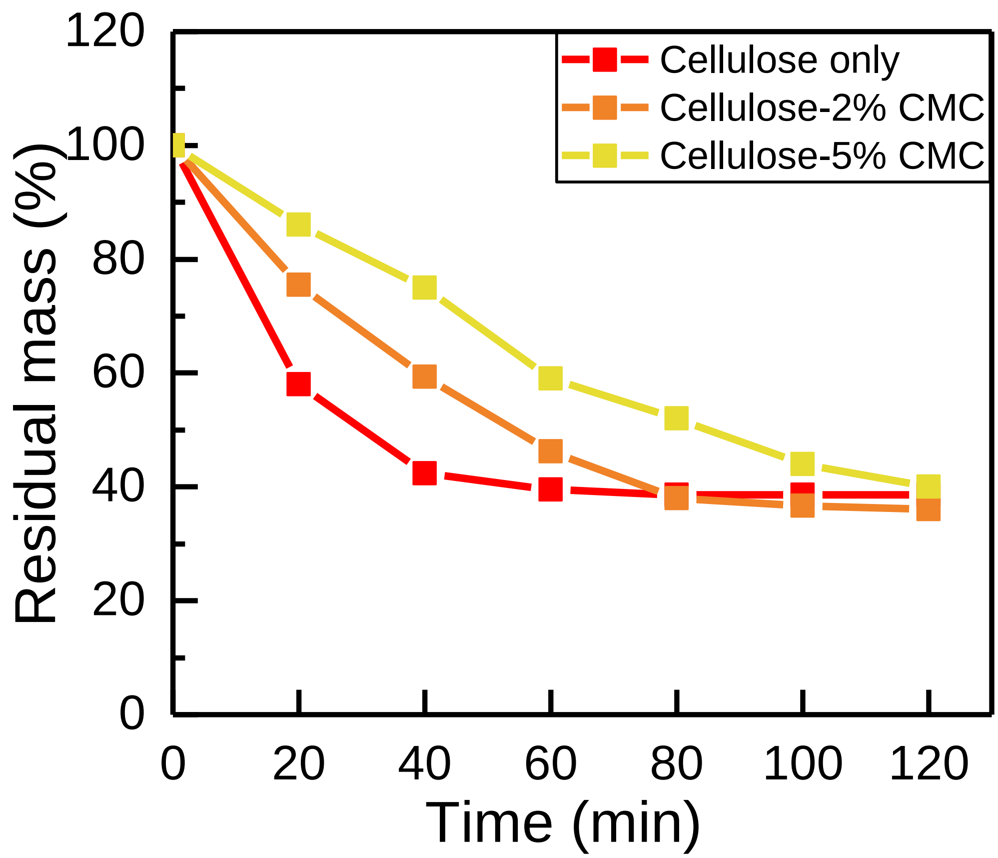


**Figure S12.** Residual mass ($Mass_{(t)}/Mass_{(t0)}$) of the different cellulose-CMC membranes (0–5 wt% CMC) as a function of time. The ambient temperature was 25 °C and the relative humidity was fixed at 1%.

**Table S2.** Water uptake of the different cellulose-CMC membranes (0–5 wt% CMC).

| Wt% of CMC | 0% | 2% | 5% |
|---|---|---|---|
| Water uptake | 159 ± 5% | 178 ± 6% | 194 ± 5% |

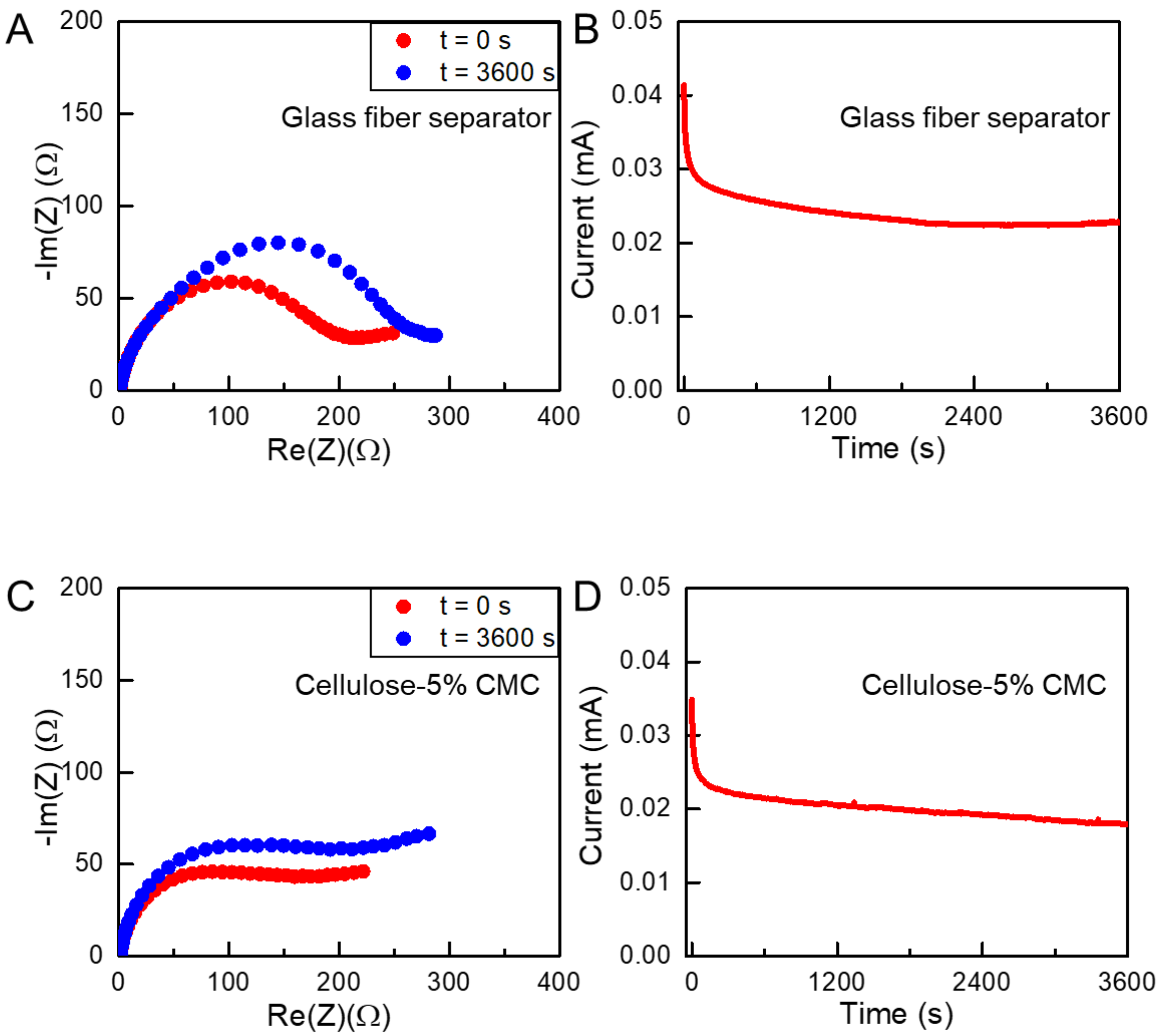


**Figure S13.** EIS of the (A) glass fiber separator and (C) cellulose-5% CMC electrolyte. The corresponding DC polarization curves with 10 mV bias of the (B) glass fiber separator and (D) cellulose-5% CMC electrolyte.

**Table S3.** Parameters measured by DC polarization and EIS for the $Zn^{2+}$ transference number.

| | $I_0$ (mA) | $I_{SS}$ (mA) | $R_0$ (Ω) | $R_{SS}$ (Ω) | t |
|---|---|---|---|---|---|
| Glass fiber | 0.041 | 0.023 | 173 | 231 | 0.33 |
| Cellulose-5% CMC | 0.035 | 0.018 | 138 | 174 | 0.39 |

$I_0$: initial current; $I_{SS}$: steady-state current; $R_0$: initial resistance; $R_{SS}$: steady-state resistance; t: transference number

**Table S4.** Relative XRD intensities $I_{002}/I_{101}$.

| Pristine Zn | Aqueous electrolyte | Cellulose-5% CMC |
|---|---|---|
| 27.26% | 27.62% | 47.50% |

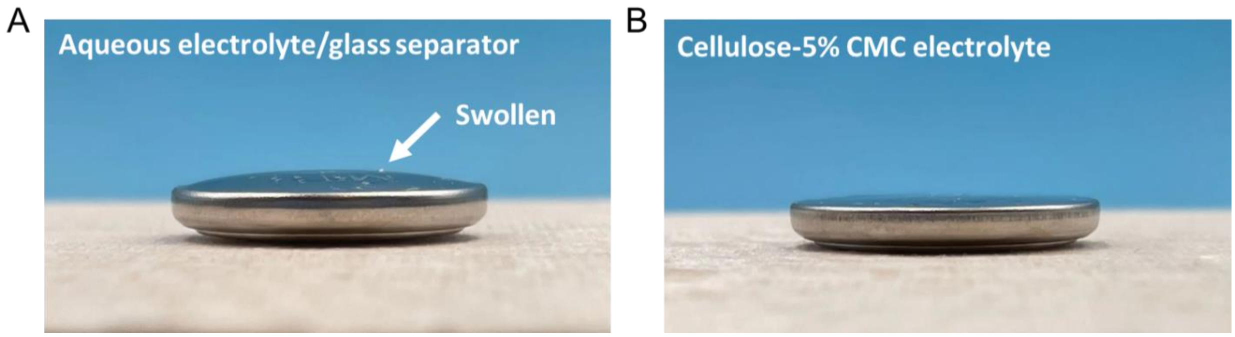


**Figure S14.** Digital images of the Zn||Zn symmetric cell (A) after 160 cycles with the aqueous electrolyte and glass fiber separator and (B) after 350 cycles with the cellulose-5% CMC electrolyte. We hypothesize the observed swelling of the coin cell using the aqueous electrolyte/glass separator was due to the hydrogen evolution reaction, while the cellulose-CMC does not show this effect.

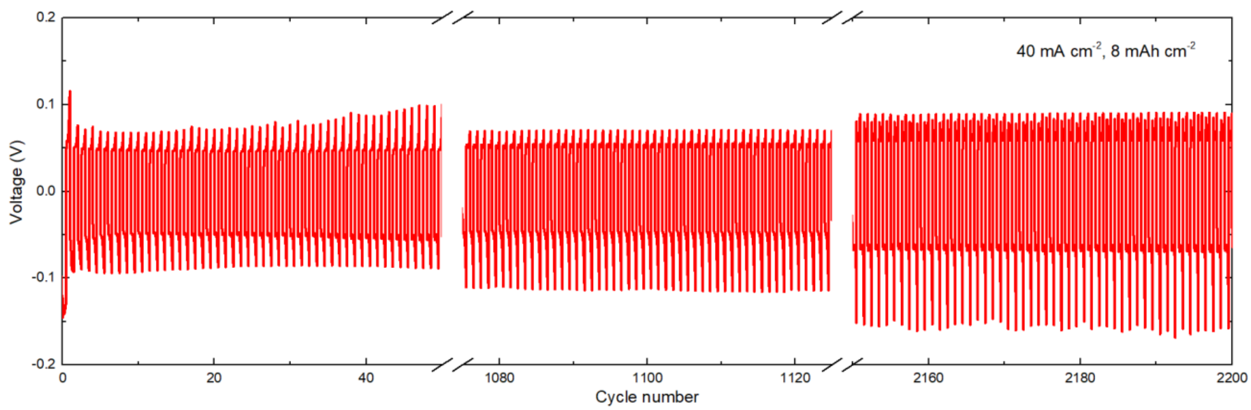


**Figure S15.** The Zn plating/stripping of a Zn||Zn symmetric cell at 40 mA/cm$^2$ and 8 mAh/cm$^2$ using the cellulose-5% CMC electrolyte.

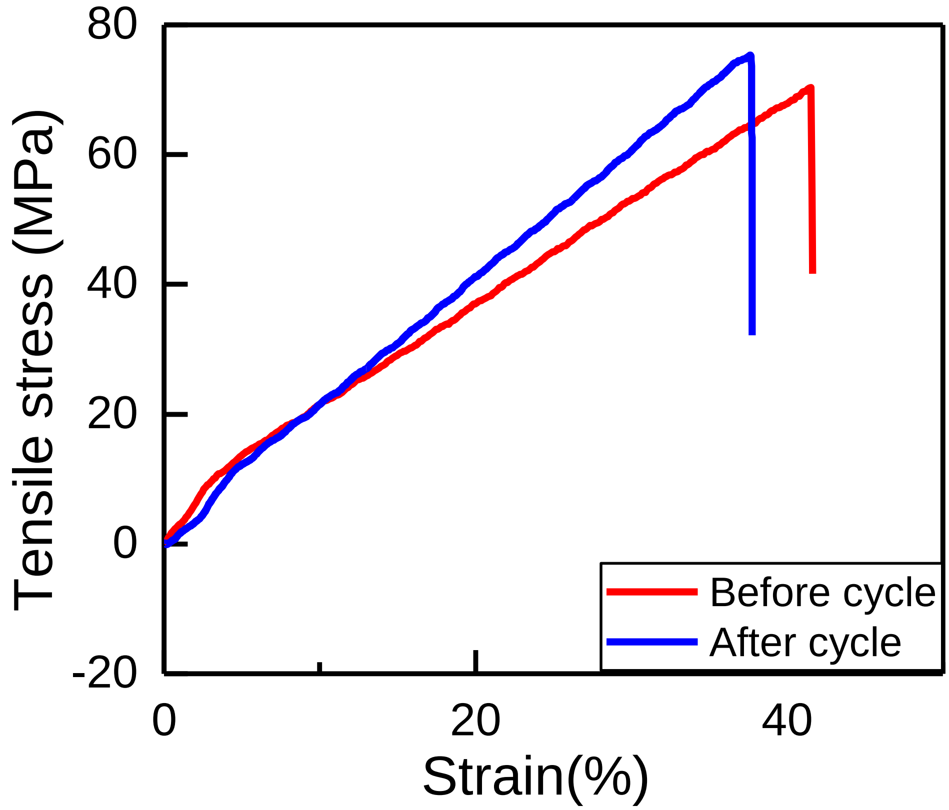


**Figure S16.** Tensile tests of the cellulose-5% CMC electrolyte before and after 3400 Zn||Zn cycles at 80 mA/$cm^2$.

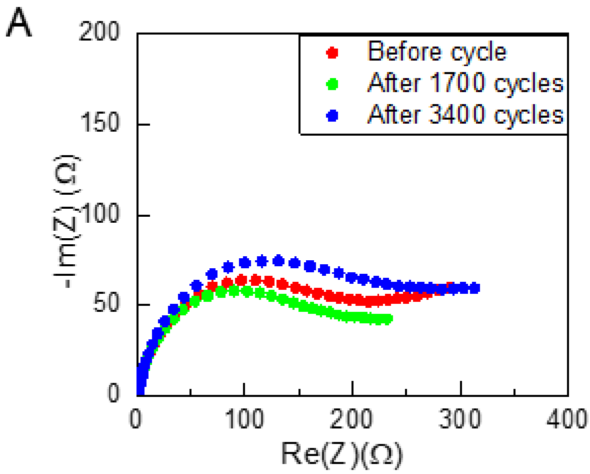


**Figure S17.** (A) EIS of a Zn||Zn symmetric cell using the cellulose-5% CMC electrolyte before cycling, after 1700 cycles, and after 3400 cycles, with a current density and capacity density of 80 $mA/cm^2$ and 4 mAh, respectively. (B) zoom-in view for the x-intercepts.

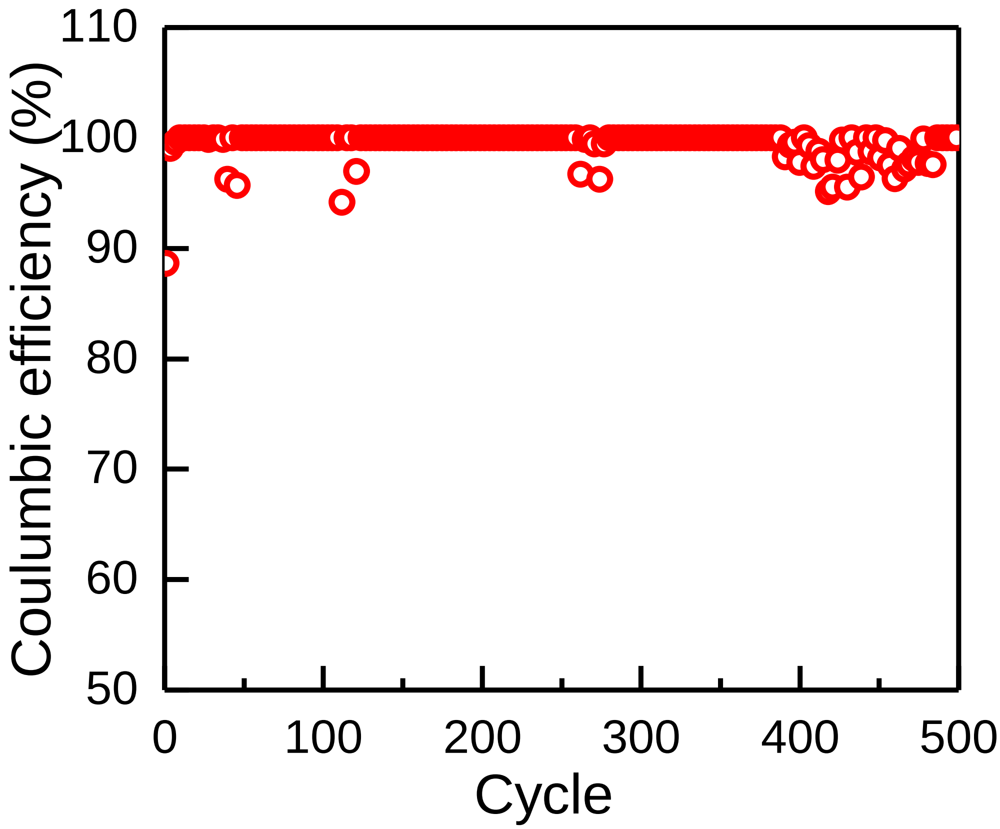


**Figure S18.** Coulombic efficiency of the Zn||Cu asymmetric cell using the cellulose-5% CMC electrolyte at 10 mA/cm$^2$ and 2 mAh/cm$^2$. The fluctuation during >400 cycles is likely due to the inevitable dendrite formation on Cu, although it is already suppressed comparing to aqueous electrolyte.

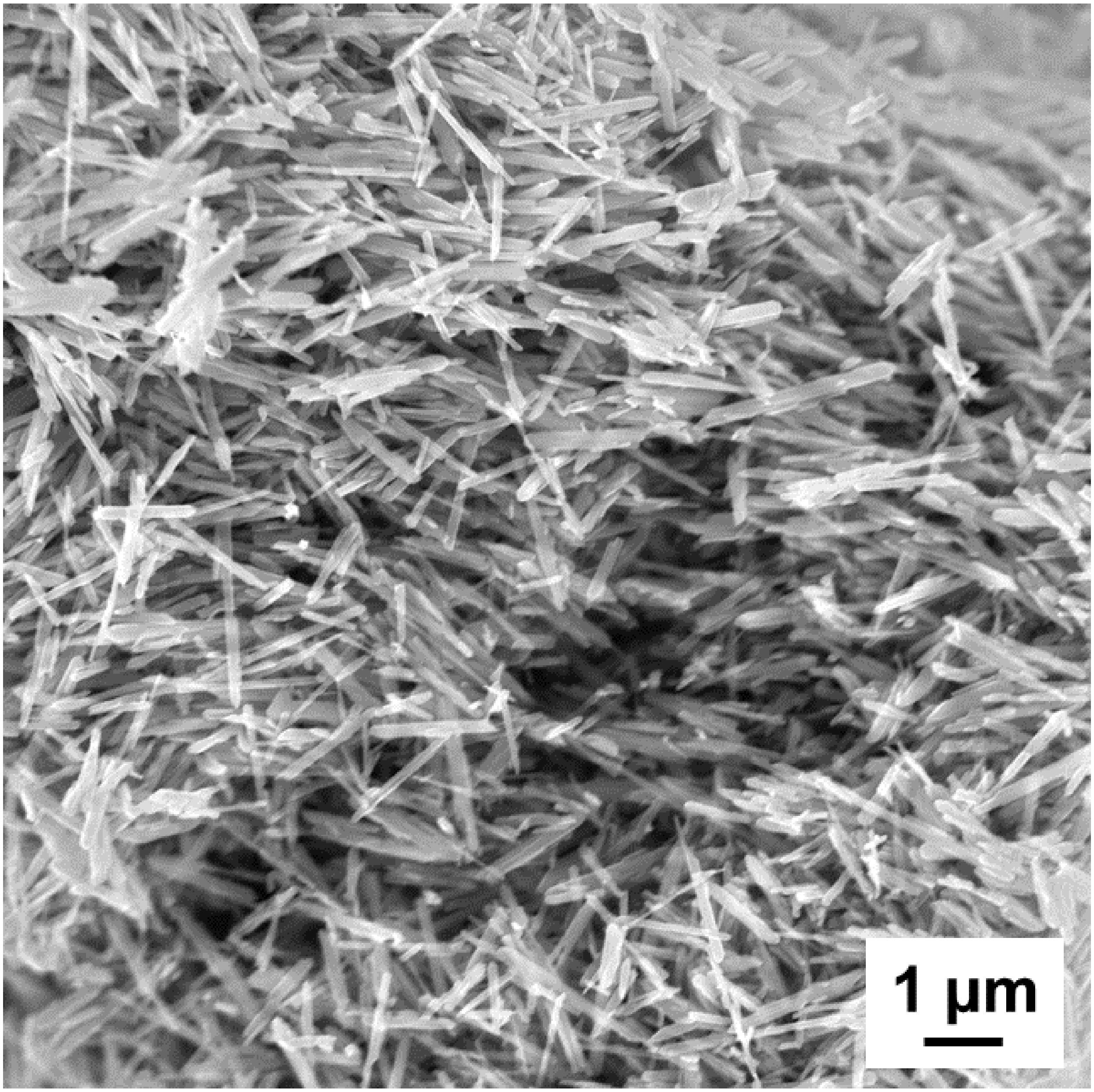


**Figure S19.** SEM image of the $MnO_2$ nanorods synthesized using a hydrothermal method.

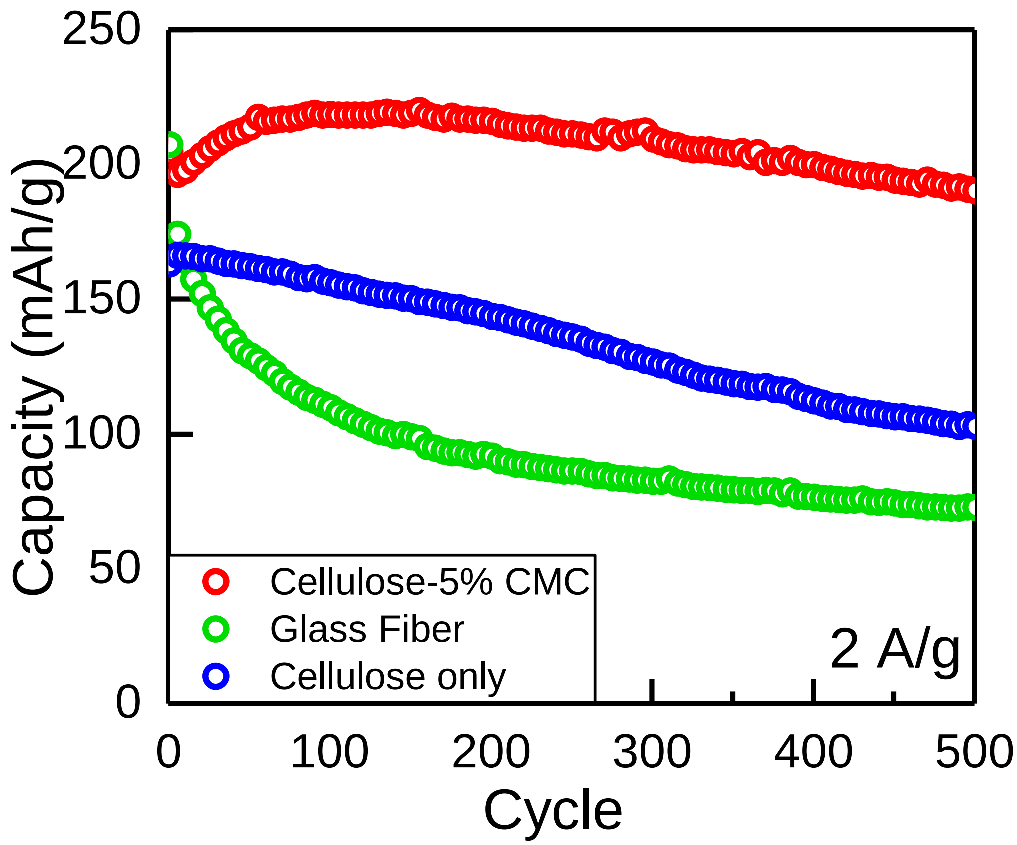


**Figure S20.** Cycling performances of Zn||$MnO_2$ cells made using the cellulose-5% CMC electrolyte, cellulose-only electrolyte (0% CMC), and aqueous electrolyte with a glass fiber separator at 8C.

**Table S5**. A short summary of the cycling performance of previously reported bio-based electrolytes for ZIBs.

| **Bio-material** | **Cathode** | **Cycle time** | **Capacity retention** | **Current density** | **Ref.** |
|---|---|---|---|---|---|
| **This Work** | **$MnO_2$** | **500 cycles** | **95%** | **2 A/g** | |
| Densified chitosan-Zn membrane | poly(benzoquinonyl sulfide) (PBQS) | 400 cycles | 71% | 4 $mA/cm^2$ | 1 |
| Nanoporous cellulose paper@glass fiber separator | $NH_4V_4O_{10}$ | 850 cycles | 89% | 4 A/g | 2 |
| Cellulose nanofiber-PAM hydrogel | $Mg_{0.23}V_2O_5 \cdot 1.0 H_2O$ | 180 cycles | 81.7% | 500 mA/g | 3 |
| Hydrogel reinforced cellulose paper | $MnO_2$ | 500 cycles | / | 200 mA/g | 4 |
| Cellulose nanofibers-$ZrO_2$ composite separator | $MnO_2$/graphite | 3000 cycles | 87.2% | 2.5 A/g | 5 |
| Cellulose aerogel-gelatin solid electrolyte | $MnO_2$ nanorod/rGO | 100 cycles | ~75% | 61.6 mA/g | 6 |
| Cellulose nanofiber zinc sulfonate membrane | $I_2$@C | 1000 cycles | 80% | 200 mA/g | 7 |

| | | | | | |
|---|---|---|---|---|---|
| Cotton-derived cellulose film | $\alpha$-$MnO_2$ | 1000 cycles | 63.6% | 1 A/g | 8 |
| Bamboo cellulose membrane | $MnO_2$ | 1000 cycles | / | 1 A/g | 9 |
| Commercial weighing paper interlayer | $V_2O_5$ | 1000 cycles | / | 0.5 A/g | 10 |

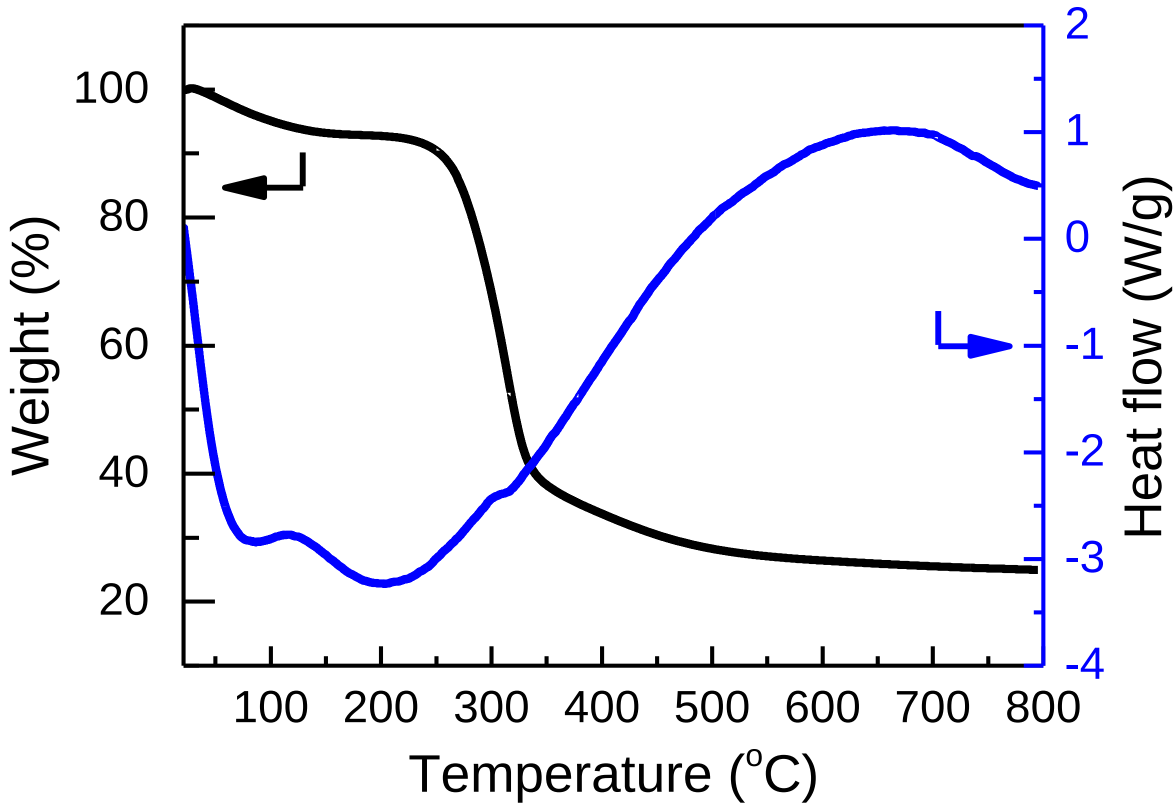


**Figure S21.** TG-DSC curve of the cellulose-5% CMC electrolyte. The cellulose-CMC membrane is stable until 250 °C. The weight loss around 100 °C is because of the loss of water. No significant exothermic peak was observed below 500 °C in the DSC curve, suggesting the low risk of thermal runaway.

# References:

[1] M. Wu, Y. Zhang, L. Xu, C. Yang, M. Hong, M. Cui, B. C. Clifford, S. He, S. Jing, Y. Yao, L. Hu, Matter 2022.
[2] Z. Yang, W. Li, Q. Zhang, C. Xie, H. Ji, Y. Tang, Y. Li, H. Wang, Mater. Today Energy 2022, 28, 101076.
[3] W. Xu, C. Liu, Q. Wu, W. Xie, W. Y. Kim, S. Y. Lee, J. Gwon, J. Mater. Chem. A 2020, 8, 18327.
[4] P. Yang, J. Li, S. W. Lee, H. J. Fan, Adv. Sci. 2022, 9, 1.
[5] J. Cao, D. Zhang, C. Gu, X. Zhang, M. Okhawilai, S. Wang, J. Han, J. Qin, Y. Huang, Nano Energy 2021, 89, 106322.
[6] J. Zhou, R. Zhang, R. Xu, Y. Li, W. Tian, M. Gao, M. Wang, D. Li, X. Liang, L. Xie, K. Liang, P. Chen, B. Kong, Adv. Funct. Mater. 2022, 32, 1.
[7] X. Ge, W. Zhang, F. Song, B. Xie, J. Li, J. Wang, X. Wang, J. Zhao, G. Cui, Adv. Funct. Mater. 2022, 32, 1.
[8] W. Zhou, M. Chen, Q. Tian, J. Chen, X. Xu, C. P. Wong, Energy Storage Mater. 2022, 44, 57.
[9] J. Fu, H. Wang, P. Xiao, C. Zeng, Q. Sun, H. Li, Energy Storage Mater. 2022, 48, 191.
[10] Y. Guo, W. Cai, Y. Lin, Y. Zhang, S. Luo, K. Huang, H. Wu, Y. Zhang, Energy Storage Mater. 2022, 50, 580.